Soft Matter

PAPER

View Article Online
View Journal | View Issue

Cite this: *Soft Matter*, 2026, **22**, 747

Tuning the velocity of thermophoretic microswimmers with thermo-sensitive polymers

Franziska Braun, Aritra K. Mukhopadhyay, Samad Mahmoudi, Kevin Gräff, Atieh Razavi, Carina Schneider, Sierk Lessnau, Benno Liebchen and Regine von Klitzing *

Understanding and controlling the motion of self-propelled particles in complex fluids is crucial for applications in targeted drug delivery, microfluidic transport, and the broader field of active matter. Here, we investigate the thermophoretic self-propulsion of partially gold-coated polystyrene Janus particles (Au–PS) in temperature-responsive linear poly(*N*-isopropyl acrylamide) (PNIPAM) solutions across various concentrations and temperatures. Particle velocities are examined at three representative temperatures: room temperature ((21 ± 0.2) °C), (28 ± 1) °C (just below the LCST), and (34 ± 1) °C (above the LCST). Viscosity values of the PNIPAM solutions were found to be close to those of pure water, with no significant shear thinning or other viscoelastic effects observed under relevant experimental conditions. In pure water, Au–PS Janus particles propel with the PS hemisphere leading, driven by their intrinsic thermophoretic response. At low polymer concentrations (0.05 wt%), experiments and theoretical calculations reveal a non-monotonic dependence of particle velocity on temperature, with a maximum near the LCST. In this regime, the positive Soret coefficient of PNIPAM causes the polymer to accumulate near the cooler PS hemisphere, generating a diffusiophoretic drift that can dominate the intrinsic thermophoretic motion and reverse the propulsion direction. Experimentally, the propulsion direction switches from PS-forward to Au-forward between 0.04 wt% and 0.05 wt%, and within the 0.05 wt% solution, a secondary reversal back to PS-forward is observed at higher temperatures, consistent with the weakening of the depletion-induced drift above the LCST. At higher concentrations (0.5 wt% and 1 wt%), the increased polymer content leads to stronger adsorption onto the entire particle surface, which suppresses propulsion by reducing local asymmetry. At 34 °C, thermophoretic propulsion stops, leaving only Brownian motion. Additionally, the diffusion coefficient increases due to temperature raise. These results highlight the potential of thermo-responsive polymers to control microswimmer dynamics, offering tunable transport properties for applications in active matter and targeted delivery systems.

Received 9th November 2025,
Accepted 15th December 2025

DOI: 10.1039/d5sm01119a

rsc.li/soft-matter-journal

Introduction

Janus particles, named after the two-faced Roman god Janus, possess distinct chemical or physical properties on their opposite sides. Over the past two decades, they have attracted significant attention due to their potential applications in various fields, including emulsion stabilization,[1,2] biological research,[3–5] and targeted cargo transport.[6–9]

A particularly intriguing class of Janus particles are self-propelling particles, which can move autonomously under specific environmental conditions. The most widely studied propulsion mechanisms include self-diffusiophoresis,[10,11] self-electrophoresis,[12] and self-thermophoresis.[13–17] Self-diffusiophoretic particles, such as platinum–polystyrene[10,11] (Pt–PS) Janus particles, generate movement through local concentration gradients of solutes, while self-electrophoretic particles, like platinum–gold[12] (Pt–Au) Janus particles, rely on self-induced electrical fields. Both mechanisms require an external chemical fuel, and propulsion ceases once the fuel is depleted. In contrast, self-thermophoretic Janus particles, like gold–coated polystyrene (Au–PS), generate propulsion by converting absorbed light into a temperature gradient, allowing precise, on-demand control *via* illumination and making them attractive for applications where chemical fuels are undesirable.

Self-thermophoretic propulsion has been primarily studied in Newtonian fluids such as water. However, many biological microswimmers like bacteria and sperm naturally navigate through viscoelastic polymeric environments, such as mucus or the extracellular matrix. These complex fluids can drastically influence propulsion characteristics, depending on both the

Soft Matter at Interfaces (SMI), Institute for Physics of Condensed Matter, Technical University of Darmstadt, Darmstadt, Germany.
E-mail: klitzing@smi.tu-darmstadt.de

swimmer type and the fluid properties. As such, understanding swimmer behavior in these environments is crucial for applications in biological and biomedical contexts. To mimic and eventually complement the functionality of biological microswimmers, artificial microswimmers have been developed. Investigating their dynamics in complex, polymeric fluids is essential for advancing their applicability in real-world environments such as targeted drug delivery or microscale transport in biological tissue. A growing body of experimental and computational studies has explored how polymeric media can either hinder or enhance swimming speed, efficiency, and hydrodynamic interactions, revealing the intricate interplay between swimmer activity and medium structure.[18–20]

A number of studies have reported that polymeric environments tend to suppress microswimmer motion. For example, Raman *et al.*[21] observed significant motility suppression of self-diffusiophoretic SiO_2–Pt Janus colloids in dilute poly(ethylene oxide) (PEO) solutions. With increasing PEO concentration, particle motion shifted from smooth to jittery and eventually to an arrested state. This suppression was attributed to anisotropic PEO adsorption onto the colloids, which altered the local viscoelastic properties and generated random stresses that hindered active motion. Similarly, computational work by Samanta *et al.*[22] demonstrated that Janus tracers (a larger sphere partially covered by smaller spheres) experienced reduced mean squared displacement (MSD) in the presence of repulsive or sticky polymers, with stronger interactions leading to more pronounced hindrance. Yadav *et al.*[23] extended this understanding by simulating self-propelled tracers interacting with long polymer chains. Increased tracer-polymer stickiness led to frequent binding events and decreased mobility, though high self-propulsion speeds allowed partial escape from adhesive effects.

In contrast, other studies have shown that viscoelastic fluids can enhance microswimmer performance. Early experimental observations demonstrated that bacteria such as *E. coli* swam faster in viscous gel-forming fluids (*e.g.*, polyvinyl pyrrolidone or methylcellulose solutions) compared to water.[24,25] This behavior may arise from microstructural effects such as pore-size filtering[25,26] or localized viscosity reduction due to flagellar rotation.[27] Patteson *et al.*[28] found that even small amounts of polymer (polyethylene glycol, carboxy-methyl cellulose, and xanthan gum) reduced *E. coli* tumbling and increased velocity, leading to enhanced translational diffusion and reduced rotational diffusion. Similarly, Smith *et al.*[29] showed that sperm achieved greater displacement per beat in viscoelastic fluids (based on supplemented Earle's Balanced Salt Solution without phenol red, containing energy substrates and various amounts of methyl cellulose solution). Teran *et al.*[30] provided theoretical support for this enhancement, showing that elastic stresses generated in the fluid could assist propulsion. Further computational studies confirmed these findings for model swimmers, including self-propelled dimers[31] and swimmers with specific propulsion gaits.[32]

Artificial microswimmers can also benefit from viscoelastic media. Schamel *et al.*[33] demonstrated that silica-based "nanoscrews" with embedded Ni segments achieved increased propulsion in viscoelastic hyaluronan gels. This enhancement is attributed to the microscopic structure of the polymer network, which facilitates propulsion and helps the nanoscrews overcome thermal noise, unlike in water where thermal fluctuations dominate and prevent directed motion. In another study, silica particles half coated with 500 nm carbon caps showed velocity-dependent trajectory changes in a viscoelastic fluid composed of water, propylene glycol propyl ether, and 0.05% polyacrylamide. At low propulsion speeds, particles moved along straight paths, while at higher speeds, frequent turning occurred due to coupling between swimmer motion and the fluid's microstructural relaxation, a phenomenon not present in Newtonian media.

Together, these studies underscore the complex and often non-intuitive effects of polymeric environments on microswimmer dynamics. While the motion of biological microswimmers in such fluids has been widely explored experimentally, and artificial swimmers have been addressed in simulations, only a limited number of experimental investigations have focused on tuning the velocity of artificial microswimmers in polymer solutions. Further work in this direction is essential for designing efficient propulsion strategies in biologically relevant, viscoelastic environments.

In this study, we aim to investigate how the velocity of artificial microswimmers can be tuned in polymer solutions. We expect a mutual interaction between self-thermophoretic microswimmers and temperature-responsive solutions. As a temperature-responsive polymer for the solutions, we choose linear poly(*N*-isopropyl acrylamide) (PNIPAM), which has a lower critical solution temperature (LCST) of around 31 °C[34]–32 °C[35–39] in aqueous solution. Below the LCST, PNIPAM adopts a swollen, hydrated coil structure, stabilized by hydrogen bonding with water.[36,37,40,41] As the temperature rises, these hydrogen bonds weaken, causing partial dehydration and a collapse into a globular structure.[35–37,41] Above the LCST, hydrophobic forces dominate, leading to polymer aggregation and phase separation due to entropy-driven dehydration.[38,40,42,43]

In this study, we systematically investigate the effects of temperature and solution concentration on the thermophoretic velocity and the diffusion coefficient of self-thermophoretic Au–PS Janus particles. The self-propulsion behavior of the Au–PS Janus particles is investigated using dark-field microscopy (DFM), while particle morphology and composition are characterized by scanning electron microscopy (SEM) and energy-dispersive X-ray spectroscopy (EDX). The temperature-dependent viscosity of the solutions is determined using rheological measurements. In the discussion, we examine how polymer concentration and the temperature-dependent thermodiffusion of PNIPAM shape the balance between intrinsic thermophoresis, polymer-induced diffusiophoresis, and adsorption-driven effects, and how this balance explains the measured thermophoretic velocities and diffusion coefficients across the three representative temperatures ((21 ± 0.2) °C), just below ((28 ± 1) °C) the lower critical solution temperature (LCST) of PNIPAM, and above ((34 ± 1) °C) the (LCST). Our

results show that at low PNIPAM concentrations (0.05 wt%), the thermophoretic velocity of the Janus particles is significantly enhanced compared to pure water, reaching a maximum just below the LCST at 28 °C. In this regime, the positive Soret coefficient of PNIPAM causes the polymer to migrate toward the cooler PS hemisphere, generating a diffusiophoretic drift that can dominate the intrinsic thermophoretic motion responsible for PS-forward propulsion in pure water. This additional drift can reverse the propulsion direction and yields the observed transition from PS-forward to Au-forward motion between 0.04 and 0.05 wt%. At higher temperatures within the 0.05 wt% solution, the depletion-induced drift weakens because the Soret coefficient drops above the LCST, resulting in a secondary reversal back to PS-forward motion. These findings are in excellent agreement with theoretical calculations modeling the combined effects of thermophoresis, polymer-induced diffusiophoresis, and the temperature-dependent Soret coefficient.

In contrast, higher polymer concentrations (0.5 wt% and 1 wt%) lead to a substantial reduction in propulsion efficiency, with thermophoretic motion completely suppressed above the LCST at 34 °C. This behavior is attributed to increased polymer adsorption and aggregation, which alter the local temperature gradient and thermo-osmotic flow around the particles. Additionally, the diffusion coefficient increases with temperature but slightly decreases with higher polymer concentrations due to elevated viscosity and polymer–particle interactions. These findings underline the potential of employing thermo-responsive polymer solutions to actively tune microswimmer dynamics through controlled adjustments of temperature and polymer concentration.

Experimental details

Materials

Polystyrene (PS) particles with a diameter of 2.39 μm were obtained from microparticles GmbH (Berlin, Germany) as 10 w/v% aqueous suspension. Linear poly(*N*-isopropyl acrylamide) (PNIPAM, M_n = 47 687 g mol^{-1}) was purchased from Merck (Darmstadt, Germany). Microscope slides (LABSOLUTE, pure white, 76 mm × 26 mm × 1 mm) were acquired from Th. Geyer GmbH + Co. KG (Renningen, Germany), while microscope cover glasses (18 mm × 18 mm) were purchased from Paul Marienfeld GmbH + Co. KG (Lauda-Königshofen, Germany). Silicon paste (Baysilone-Paste) for sealing was obtained from Carl Roth GmbH + Co. KG (Karlsruhe, Germany). Ethanol was acquired from Fisher Chemical (Waltham, USA). Deionized water (resistance 18.2 MΩ cm at 25 °C) was provided by a MilliQ water purification system from Merck (Darmstadt, Germany).

Au–PS particle preparation

Gold-coated polystyrene particles (Au–PS) were produced *via* thermal evaporation. The Langmuir–Blodgett technique[44,45] was employed to transfer a monolayer of PS particles onto microscope slides. A 5 nm chromium layer was then deposited on the exposed surface of the particles, followed by a 50 nm Au layer applied on top of the chromium. The thermal evaporation was carried out using a CREAMET 300 V2 device. For a more comprehensive description of the preparation process for the Janus particles, refer to Braun *et al.*[15]

Table S1 in the SI summarizes the parameters used in the thermal evaporation process. During coating, the thickness of the metal layer was monitored using a built-in quartz crystal microbalance. Once prepared, the Janus particles were detached from the glass substrate by adding MilliQ water.

Characterization techniques

SEM. Scanning electron microscopy (SEM) of the Janus particles was conducted using a Gemini 500 field emission scanning electron microscope (FESEM) from Carl Zeiss (Oberkochen, Germany). This instrument also enables elemental analysis through energy-dispersive X-ray spectroscopy (EDX), allowing the mapping of the Au and the PS regions of the Janus particles. An SEM image and the corresponding EDX analysis of an Au–PS particle can be found in the SI in Fig. S1.

Self-propulsion measurements. To prepare the sample cell for the self-propulsion measurements (see Fig. 1, inset), a 1 μL droplet of the Au–PS particle dispersion is placed between two bare glass slides (18 × 18 mm^2), which were pre-cleaned in ethanol using an ultrasonic bath for 30 min. The edges of the glass slides were sealed with silicon paste to prevent water evaporation inside the sample cell and to restrict particle movement to the *xy*-plane. The distance between the two glass slides was approximately 15 μm, corresponding to several particle diameters. The sample cell is mounted onto the objective, and by coupling a laser into the system, the self-propulsion behavior of the Janus particles is triggered and can be observed. Here, local laser heating of the gold cap leads to a temperature rise of a few kelvin, consistent with previous reports by Jiang *et al.*,[13] Bickel *et al.*,[46] and Bregulla *et al.*[16]

Self-propulsion measurements are carried out using a home-built dark-field microscope setup (schematically depicted in Fig. 1, top). A dark-field condenser (Olympus, NA 1.2–1.4) enables an enhanced detection of the Au cap. The scattered light from the particles in the sample cell is collected with an oil-immersion objective (Olympus 100×, adjustable NA 0.5–1.35) and recorded using an sCMOS camera (Andor, Zyla 4.2). A green laser (Pegasus, Pluto, 800 mW) with a wavelength of 532 nm is coupled into the microscope to stimulate the self-propulsion of the Au–PS particles. A nano-positioning stage (P-545.2R7) maintains the particle within the illumination area. A feedback loop adjusts the stage position as needed, while a LabVIEW program tracks *x*- and *y*-positions in real time. Further details are available in Heidari *et al.*[14,47]

For times much shorter than the rotational diffusion time $\tau_r = 1/D_r = (8\pi\eta R^3)/(k_B T) \approx 10$ s, where η is the viscosity of water, R is the particle radius, and $k_B T$ is the thermal energy, the lateral mean squared displacement (MSD) follows:[10,48,49]

$$\mathrm{MSD} = 4D_{\mathrm{meas}}t + v_{\mathrm{th}}{}^2 t^2, \quad (1)$$

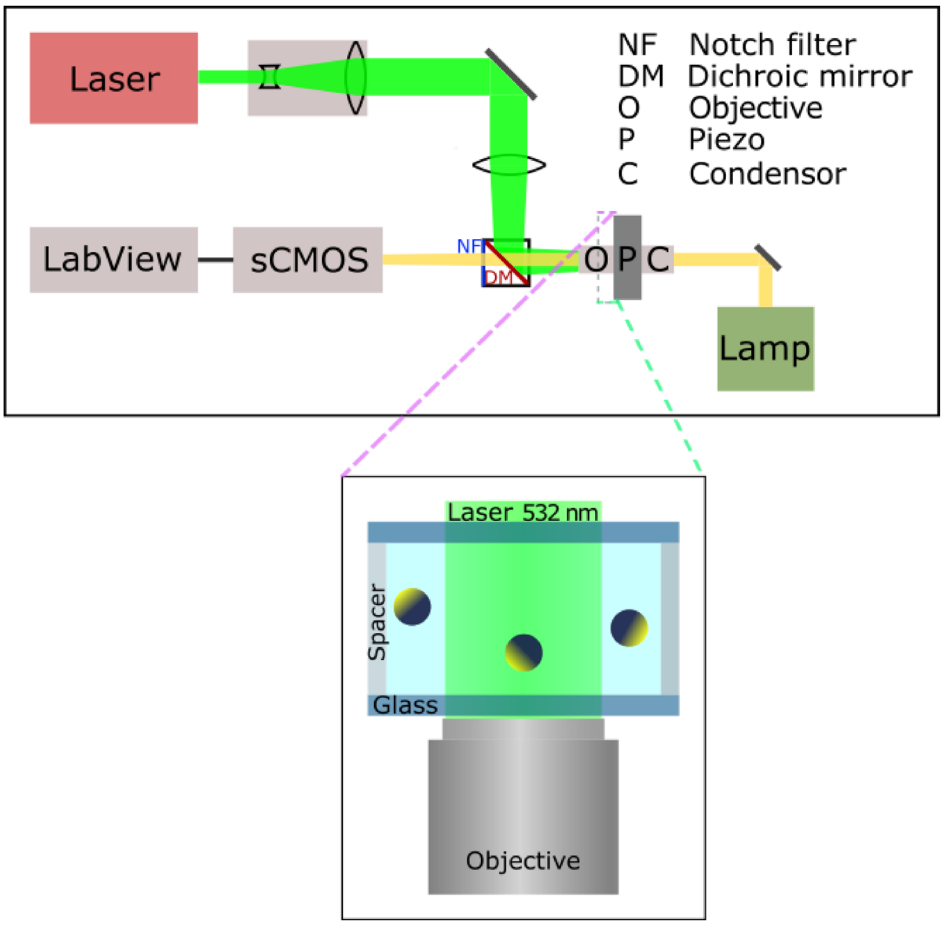

Fig. 1 Dark-field microscopy setup with a magnified view of the sample cell. To produce a wide parallel beam at the sample location, the laser beam passes sequentially through a beam expander and a lens. The sample cell is positioned on a nano-positioning stage above the objective, and the Janus particle is imaged using a camera.

where v_{th} is the thermophoretic velocity of a particle and t is the lag time. By fitting the experimental MSD curves (see Fig. S2–S6, SI) with equation 1, we extract the diffusion coefficient D_{meas} (see below and Fig. S7 and S8 in the SI) and the thermophoretic velocity v_{th} (see below). Measurements are conducted near a glass substrate, with an estimated particle–substrate distance of 200–300 nm[50] in water. The error bars indicate the standard deviation from at least 40–50 measurement values per data point.

The diffusion coefficients D_{meas} are compared to the diffusion coefficient in bulk D_{bulk}:[51]

$$D_{bulk} = \frac{k_B T}{6\pi\eta R} \quad (2)$$

with (temperature-dependent) fluid viscosity η and particle radius R.

Self-propulsion measurements with sample heating. The self-propulsion measurements were conducted at three different temperatures. First, at room temperature of (21 ± 0.2) °C. Second, at a temperature (28 ± 1) °C, slightly below LCST (around 31 °C[34]–32 °C[35–39]) of PNIPAM. Finally, at a temperature (34 ± 1) °C, above the LCST.

To heat the sample to 28 °C and 34 °C, two heating belts were used. One heating belt was secured to the microscope objective, and the other to the condenser using cable ties. This setup allowed the sample to reach 28 °C at heating level 1 of the belts and 34 °C at heating level 2. The temperature of the sample was measured with an infrared thermometer shortly before and after each self-propulsion measurement to ensure it was at the desired temperature.

Rheology. The temperature-dependent (dynamic) viscosity of water and PNIPAM solutions with various concentrations was measured using an MCR 702 Rheometer from Anton Paar (Graz, Austria) equipped with a Peltier element for temperature control. All experiments were conducted with a double-gap geometry (DG26.7-SS). The temperature was controlled with an accuracy of ±0.2 °C.

Between the outer cylinder and the rotatable cylinder, 3.8 mL of water or the aqueous PNIPAM solutions were loaded. For the measurement protocol, a loop was programmed in the Anton Paar software to record shear stress over a range of shear rates for each temperature. The measurements were taken stepwise from 20 °C to 40 °C in 1 °C increments (and then back down to 20 °C for one solution in the same manner). The

viscosity at each temperature was determined as the ratio of shear stress to shear rate. By fitting a constant to the viscosity-shear rate curves for each temperature, a single viscosity value was obtained for each temperature (see Fig. S9 and S10, SI). The acquisition time of each temperature was 15 min before a measurement started and the timeout between two temperatures was 30 min.

Viscometer. In addition to the measurements of dynamic viscosity using a rheometer, the kinematic viscosity (see Table S2) was determined at 20 °C, 28 °C, and 34 °C using an Ubbelohde viscometer 015T from Lauda Scientific GmbH (Lauda-Königshofen, Germany). The underlying measurement principle is based on the flow of the test liquid through a narrow capillary tube. A defined volume of liquid flows under constant pressure through a capillary with a certain length an radius, and the time t required for this flow is recorded.

The kinematic viscosity ν is then calculated by multiplying the measured flow time t by the capillary constant K, which depends solely on the design of the viscometer. According to the Hagen–Poiseuille law, the kinematic viscosity ν is directly proportional to the flow time t_{flow}[52]:

$$\nu = K \cdot t_{\mathrm{flow}} \tag{3}$$

The dynamic viscosity η can then be derived from the kinematic viscosity by multiplying it with the fluid density ρ[53]:

$$\eta = \rho \cdot \nu \tag{4}$$

The fluid density at the required temperatures was determined using a DM40 Density Meter from Mettler Toledo GmbH (Gießen, Germany).

Zeta sizer measurements. The hydrodynamic radius R_{h} of the linear PNIPAM polymer in solution was measured at 21 °C at a scattering angle of 173° using a Malvern Panalytical Zetasizer NanoZ (Malvern, UK). For the measurement, a PMMA cuvette was thoroughly cleaned with ethanol and MilliQ water before being filled with a 0.05 wt% aqueous PNIPAM solution. The final value of R_{h} was determined as the average of six individual measurements.

The zeta potential of the Janus particles was measured at 21 °C to determine the sign of their surface charge. Since the particles are too large for precise measurements, the results are used qualitatively rather than quantitatively, providing insight into whether the particles are positively or negatively charged.

Additionally, the zeta potential of the Janus particles in PNIPAM solutions was measured at 20 °C, 40 °C, and again at 20 °C to assess trends indicating PNIPAM adsorption onto the particle surfaces.

Overlap concentration of PNIPAM solution. To determine whether our PNIPAM solutions are in the dilute concentration regime, we estimate the overlap concentration c^*, which marks the transition between the dilute and semidilute regimes. The overlap concentration c^* can be calculated by using[54]:

$$c^* = \frac{M_{\mathrm{w}}}{\frac{4}{3}\pi R_{\mathrm{h}}^3 N_{\mathrm{A}}} \tag{5}$$

with average molecular weight of the polymer M_{w}, hydrodynamic radius of the polymer R_{h}, and Avogadro's number N_{A}.

From the manufacturer, we only know the number-average molecular weight M_{n} of the polymer, $M_{\mathrm{n}} = 47\,687$ g mol^{-1}. Since M_{n} is always smaller than the weight-average molecular weight M_{w}, using M_{n} instead of M_{w} in eqn (5) results in a lower estimated overlap concentration c^* than the actual value. If our chosen concentration is below this lower estimate, it is certainly also below the true overlap concentration, confirming that we are in the dilute concentration regime.

The hydrodynamic radius R_{h} of the polymer was measured using a Zetasizer NanoZ and determined to be (15.7 ± 1.1) nm at 21 °C. This results in an estimated lowest overlap concentration of $c^* = 4.9$ g L^{-1}. Assuming a density of the polymer solution of about 1 g cm^{-3}, the overlap concentration would be around 0.49 wt%. However, since $M_{\mathrm{n}} < M_{\mathrm{w}}$, the actual overlap concentration should be higher than 0.49 wt%. This means that for the lowest concentration of 0.05 wt%, we are clearly in the dilute regime. For the intermediate (0.5 wt%) and highest (1 wt%) concentrations, we may be in the transition region toward the semi-dilute regime.

Results

To characterize the self-propulsion behavior of Au–PS Janus particles, we measure their thermophoretic velocities and diffusion coefficients in PNIPAM solutions of varying concentrations at different temperatures (21 °C, 28 °C, and 34 °C). In addition, we performed theoretical calculations of Janus particles in dilute PNIPAM solutions, which take the polymer's thermodiffusive response to temperature gradients into account. To better understand how the fluid properties influence particle dynamics, the temperature-dependent viscosities of water and linear PNIPAM solutions are also measured.

Thermophoretic speed

As a reference system, the thermophoretic speed of the particles is first examined in pure water at 21 °C (filled blue circles), 28 °C (open blue circles), and 34 °C (open red circles), as shown in Fig. 2(a). The speed increases approximately linearly with laser power, and no change in speed is observed with rising temperature. Fig. 2(b)–(d) summarize the thermophoretic velocities measured in the PNIPAM solutions at concentrations of (b) 0.05 wt%, (c) 0.5 wt%, and (d) 1 wt%. The filled symbols indicate 21 °C, the open blue symbols 28 °C, and the open red symbols 34 °C.

In the 0.05 wt% solution (Fig. 2(b)), the speed at 21 °C is significantly higher than in water across all laser powers. Increasing the temperature to 28 °C further increases the speed, whereas heating to 34 °C causes a drastic decrease in speed, resulting in values even lower than those in water.

For the 0.5 wt% solution, the velocities at 21 °C and 28 °C are comparable to those in water. However, at 34 °C, the behavior of the particles changes significantly, and they only

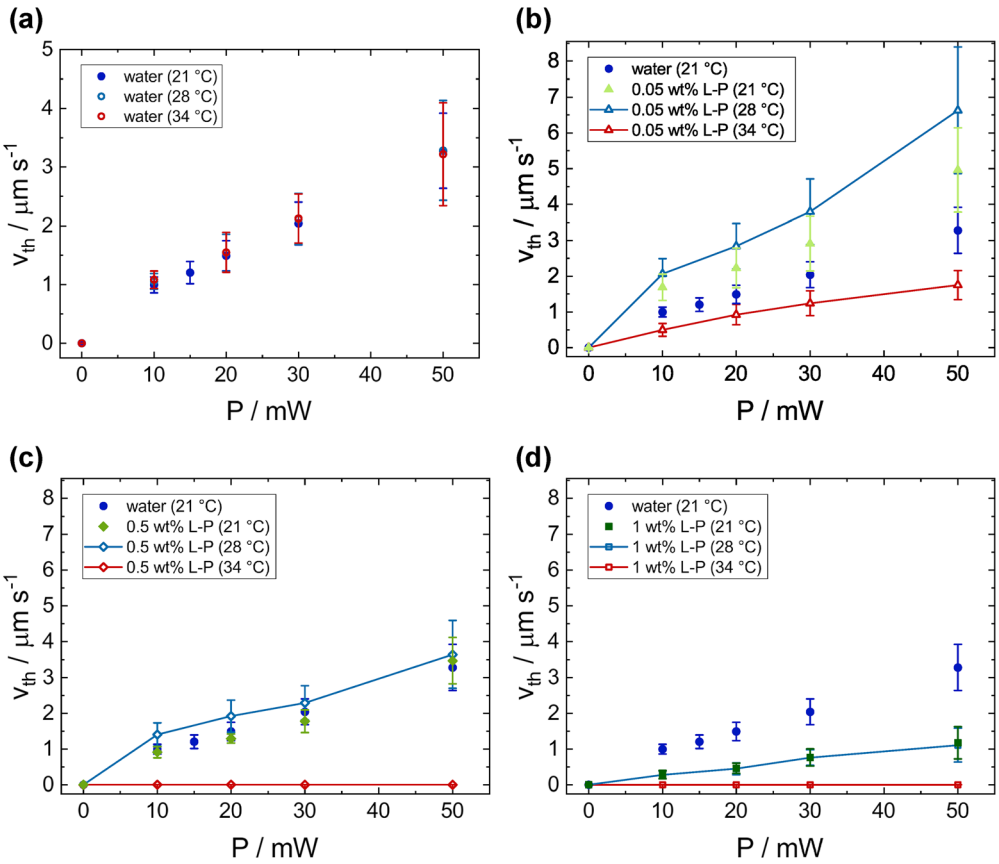

Fig. 2 Thermophoretic speed *versus* laser power for different temperatures in (a) water and in the PNIPAM solutions with various concentrations: (b) 0.05 wt%, (c) 0.5 wt%, and (d) 1 wt%. Filled symbols: 21 °C; open blue symbols: 28 °C; open red symbols: 34 °C.

exhibit Brownian motion, meaning the thermophoretic speed becomes zero.

In the 1 wt% PNIPAM solution, the velocities at 21 °C are significantly lower than in water. No speed increase is observed upon heating to 28 °C, and the values remain below those in water. At 34 °C, the thermophoretic speed becomes zero, and the particles only exhibit Brownian motion, similar to the behavior in the 0.5 wt% solution.

In the 1 wt% PNIPAM solution, the thermophoretic speed increases approximately linearly with laser power at both 21 °C and 28 °C. At lower concentrations, slight deviations from linearity appear, especially at low laser powers (*e.g.*, 10 mW), where the speed exceeds the expected linear trend. This effect is most pronounced in the 0.05 wt% solution at 28 °C but is also noticeable at 21 °C. In the 0.5 wt% solution, the deviation is less pronounced. Additionally, in the 0.05 wt% solution at 28 °C, the speed at 50 mW is slightly higher than predicted by a linear trend, whereas at 34 °C it is slightly lower.

To capture the overall trend of laser impact on the speed, a linear fit is applied to the data, although slight deviations from a linear relation between thermophoretic speed and laser power (see Fig. 2(b)–(d)) are observed. Each speed curve in Fig. 2 was fitted with a straight line constrained to pass through the origin (0,0). The resulting slope serves as a measure of the laser-induced propulsion efficiency, which is plotted in Fig. 3 as a function of temperature for the different concentrations.

The propulsion efficiency in the PNIPAM solutions reaches a maximum at temperatures slightly below the LCST, indicating that the thermophoretic speed increases most strongly with laser power in this regime. Both the absolute efficiency and the

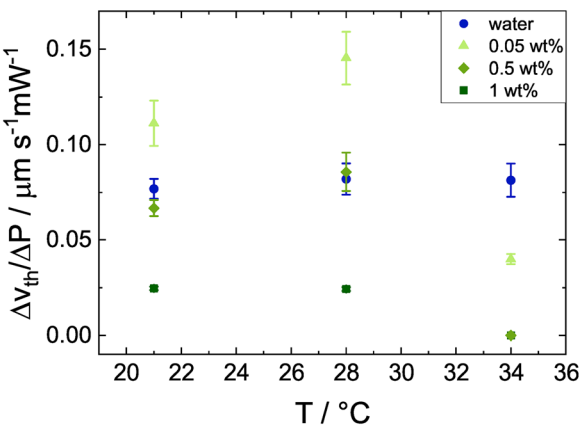

Fig. 3 Temperature dependence of laser-driven propulsion efficiency. Each point represents the slope of a linear fit to the speed *versus* laser power data in Fig. 2, constrained to pass through (0,0).

pronounced nature of this peak diminish with increasing polymer concentration. At 0.05 wt% PNIPAM, the efficiency exhibits a distinct peak slightly below the LCST. At 0.5 wt% PNIPAM, the efficiency remains somewhat higher at 28 °C than at 21 °C, while at the highest concentration of 1 wt% PNIPAM, the efficiencies at 28 °C and 21 °C become nearly identical. In all PNIPAM solutions, the efficiency drops to its lowest values at 34 °C.

In contrast, the propulsion efficiency in water remains temperature-independent. In the 0.05 wt% PNIPAM solutions, the efficiency at 21 °C and 28 °C is significantly higher than in water. In the 0.5 wt% PNIPAM solutions, the efficiency remains comparable to that of water of these temperatures. At 1 wt% PNIPAM, however, the efficiency is lower than that in water across all temperatures investigated. At 34 °C, the propulsion efficiency in all PNIPAM solutions is drastically reduced compared to water.

When plotted directly against concentration (Fig. 4), the concentration-dependent trends of the thermophoretic speed become clearer. At 21 °C (Fig. 4(a)), the velocities in the 0.05 wt% PNIPAM solution are significantly higher than in water, decreasing steadily with PNIPAM concentration and falling well below water values in 1 wt% PNIPAM solutions.

At 28 °C (Fig. 4(b)), the velocities in 0.05 wt% PNIPAM solution increase further, reaching nearly double those in water at 50 mW. As the PNIPAM concentration increases, the speed declines, though it remains slightly higher than in water at the medium concentration of 0.5 wt%. At the highest concentration of 1 wt%, the speed drops below that of water.

At 34 °C, in Fig. 4(c), increasing the PNIPAM concentration leads to a sharp decrease in speed, eventually reaching zero at 0.5 wt% and 1 wt%, indicating pure Brownian motion.

In summary, the speed of the Au–PS Janus particles in PNIPAM solutions is governed by two main parameters. First, adjusting the polymer concentration allows tuning of the speed. Adding a small amount of PNIPAM (0.05 wt%) results in a significant increase in speed, which, under certain conditions (heating to 28 °C at 50 mW), is doubled compared to the speed in water at 50 mW. Increasing the concentration of PNIPAM further, however, enables velocities below those observed in water. Second, temperature modulation influences the speed behavior. At 0.05 wt% PNIPAM, heating to 28 °C (slightly below the LCST) substantially increases the speed, whereas further heating to 34 °C (slightly above the LCST) causes a pronounced reduction. This temperature-driven effect becomes even more dominant at higher concentrations, where the velocities drop to zero at 34 °C, leaving only Brownian motion.

3.2 Prediction of velocity reversals in dilute solutions

To explain the observed velocity trends for low concentrations of PNIPAM, particularly the non-monotonic behavior, we apply a theoretical model based on the combined effects of thermophoresis and depletion forces. In the dilute 0.05 wt% PNIPAM solution, the total Janus particle velocity v_{th} can be modeled as a linear superposition of the particle's intrinsic thermophoretic velocity $\mathbf{v}_T$ and a PNIPAM-driven depletion contribution $\mathbf{v}_D$. This mechanism is analogous to that described for colloidal particles in surfactant solutions.[55] The laser-induced heating of the Au cap creates a temperature gradient in the surrounding fluid across the Janus particle, causing the PNIPAM polymer to undergo thermophoresis. This leads to a non-uniform polymer concentration field around the particle, with PNIPAM accumulation in cold regions owing to the positive Soret coefficient of PNIPAM.[56] Such a polymer gradient causes an entropic force (depletion force) pushing the swimmer from high-to-low PNIPAM concentration, *i.e.*, from the cold PS side towards the hot Au cap (see schematic in Fig. 5(c)). This results in an additional drift opposing the particle's intrinsic thermophoretic motion. The total velocity of the particle is given by the sum of these two contributions:[57,58]

$$\mathbf{v}_{th} = \mathbf{v}_T + \mathbf{v}_D = -D_T \nabla T + \frac{k_B}{3\eta} R_g^2 n (T S_T - 1) \nabla T \qquad (6)$$

where, D_T is the intrinsic thermophoretic mobility (in water) of the particle, k_B is the Boltzmann constant, η is the solvent viscosity, R_g is the polymer's radius of gyration, n is the polymer number density, T is the absolute temperature, S_T is the Soret coefficient of the polymer, and ∇T is the temperature gradient across the Janus particle. It is important to emphasize that the mechanism behind the additional drift relies on depletion interactions (entropic forces) driving the particle down the

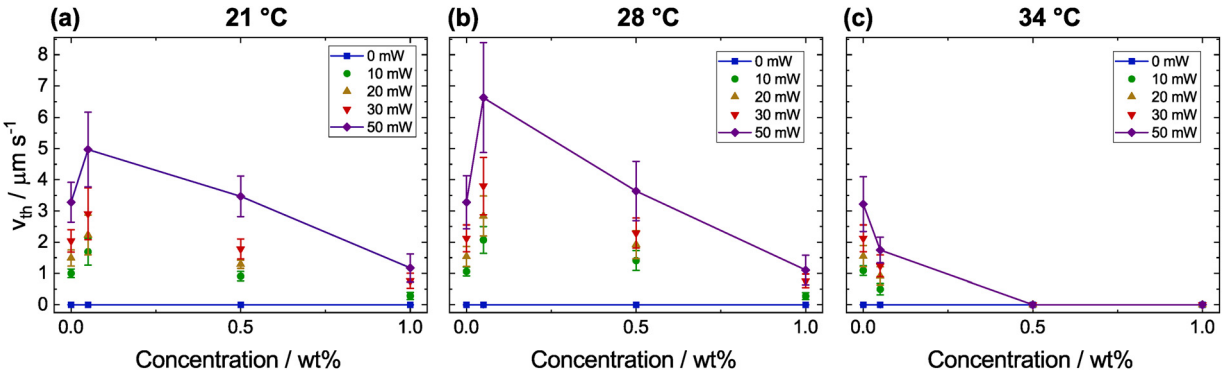

Fig. 4 Thermophoretic speed as a function of PNIPAM concentration at various laser powers at (a) 21 °C, (b) 28 °C, and (c) 34 °C.

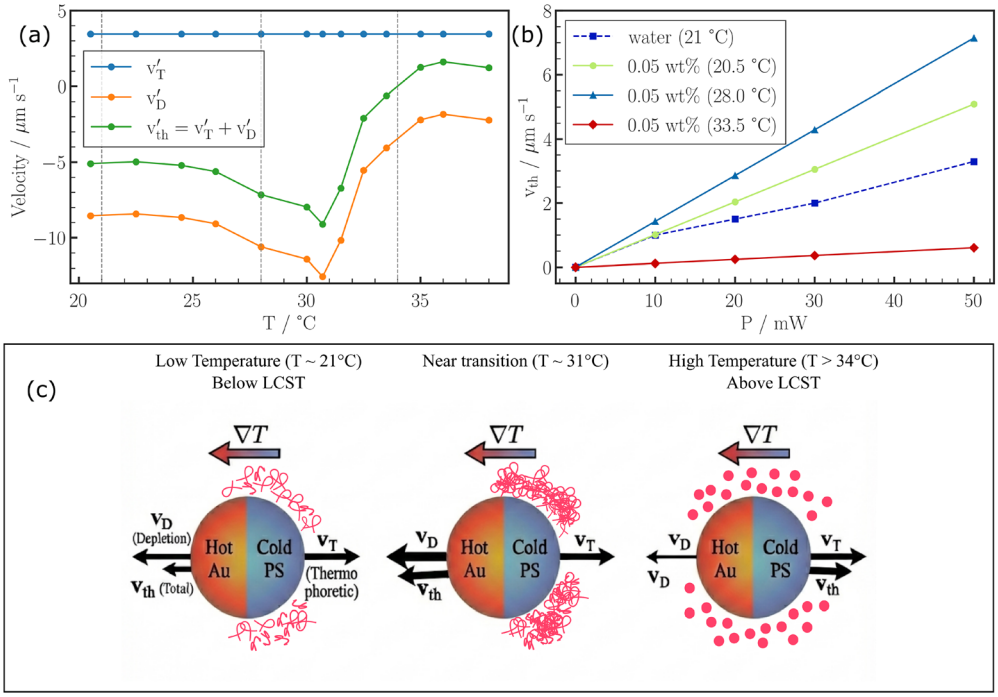

Fig. 5 (a) Predicted thermophoretic velocity in a 0.05 wt% PNIPAM solution as a function of temperature. The total velocity (v'_{th}, green) is the sum of the thermophoretic velocity (v'_T, blue) in water without PNIPAM and the additional depletion (diffusiophoretic) contribution (v'_D, orange) due to PNIPAM. A positive velocity indicates propulsion with the PS cap forward, while a negative velocity signifies Au cap-forward motion. The three dashed vertical lines correspond to the experimental temperatures of 21 °C, 28 °C, and 34 °C for the 0.05 wt% solution shown in Fig. 4. (b) Predicted speed $v_{th} = |v'_{th}|$ as a function of laser power P for the 0.05 wt% PNIPAM solution at different temperatures. The data for pure water (blue dashed line) is from experiment (Fig. 2(b)). (c) Schematic representation of the propulsion mechanism across three temperature regimes. At low temperatures and near the LCST, the strong depletion force caused by non-uniform PNIPAM (depicted in pink) concentration reverses the motion (Au-cap leading). Above the LCST, depletion effects are reduced, restoring PS-cap leading motion.

concentration gradient, which is distinct from diffusiophoresis based on diffusioosmotic flows along the particle surface.

The behavior of the depletion term $\mathbf{v}_D$ is critically dependent on the Soret coefficient S_T of PNIPAM. As reported by Kita *et al.*,[56] S_T for PNIPAM in water is positive (indicating polymer migration to the cold side) and exhibits a strongly non-monotonic dependence on temperature, peaking sharply at its coil-to-globule transition temperature ($\approx$31 °C). We extracted these temperature-dependent S_T values from Kita *et al.*[56] to numerically estimate the depletion contribution $\mathbf{v}_D$. The thermophoretic mobility of Au–PS Janus particle is taken from literature as $D_T \approx 2.35\ \mu m^2\ s^{-1}\ K^{-1}$.[59] The propulsion efficiency in pure water at laser power P is estimated by a linear fit of the particle speed $v_{th} = \epsilon P$ of the experimental data (from Fig. 2(b)), yielding $\epsilon \approx 0.069\ \mu m\ s^{-1}\ mW^{-1}$. The magnitude of the temperature gradient is then estimated from the relation $|\nabla T| = v_{th}/D_T = \epsilon P/D_T$. For the 50 mW laser power, this estimates $|\nabla T| \approx 1.47\ K\ \mu m^{-1}$.

Fig. 5(a) shows the calculated velocity components (v'_{th}, v'_T, v'_D) along the Janus particle's body-fixed unit vector, defined as pointing from the hot Au cap to the cold PS cap, as a function of temperature. Since S_T is positive (between 0.1–0.7 K^{-1} in the temperature range 20–38 °C) and the $(TS_T - 1)$ term is large, the depletion contribution v'_D is negative (orange line), indicating a strong drift that opposes v'_T and is directed towards the hot Au cap. The component of the total velocity $v'_{th} = v'_T + v'_D$ (green line) is consequently also negative for temperatures below $\approx$34 °C, predicting that the Janus particle moves with its Au cap forward in such dilute polymer solution. The speed of the particle at the three dashed vertical lines in the figure, which mark the experimental temperatures of 21 °C, 28 °C, and 34 °C, qualitatively matches with the non-monotonic velocity-temperature trend reported for the 0.05 wt% solution in Fig. 4. This non-monotonic temperature dependence is further illustrated in Fig. 5(b), which plots the predicted speed of the particle as a function of laser power near these temperatures. The model shows the particle speed is highest near the LCST (28.0 °C) and strongly suppressed above it (33.5 °C), similar to that observed in experiments (Fig. 2(b)). To account for the temperature-dependent polymer size, we further estimated the velocity contributions using the PNIPAM radii from literature, which decrease from $\approx$39 nm (21 °C) to $\approx$21 nm (38 °C) across the phase transition.[56] Comparing the depletion velocity ($\mathbf{v}_D$) to the intrinsic thermophoretic velocity ($\mathbf{v}_T$), we find that below the LCST, the depletion term dominates with a ratio of $|v'_D|/|v'_T| \approx 2.6$. Above the LCST, the simultaneous reduction in radii and Soret coefficient causes this ratio to drop to $\approx$0.27, rendering the depletion force weaker compared to the intrinsic thermophoresis. It is important to note that the depletion term v'_D in this model is directly proportional to the

PNIPAM concentration n, which explains the strong velocity enhancement in 0.05 wt% PNIPAM compared to pure water. This dilute-regime model does not, however, capture the suppression observed experimentally at higher concentrations (0.5 wt% and 1.0 wt%), where aggregation and polymer adsorption effects become dominant and inhibit self-propulsion.

3.3 Experimental observations of velocity reversals

Fig. 6 illustrates the change in propulsion direction induced by the presence of PNIPAM. In pure water at 21 °C, the Janus particles predominantly move with the PS hemisphere leading. In contrast, at the same temperature but in a 0.05 wt% PNIPAM solution, the propulsion reverses and the particle moves with the Au cap facing forward.

Importantly, as the theoretical calculations predict that Au–PS Janus particles move with the Au cap facing forward even at low PNIPAM concentrations of 0.05 wt%, we experimentally confirm this behavior. The results show that the reversal of propulsion direction occurs between 0.04 wt% and 0.05 wt%: at 0.04 wt%, the particles still move PS-forward as in pure water, whereas at 0.05 wt% they move Au-forward, in full agreement with the theoretical calculations. Moreover, within the 0.05 wt% solution, the propulsion direction itself exhibits a subtle temperature difference. While the particles move with the Au can in front at 21 °C, 28 °C, 31 °C, they reverse again at 34 °C and return to PS-forward motion, in agreement with the theoretical calculations.

Diffusion coefficients

Fig. S7 and S8 present the diffusion coefficients in water and PNIPAM solutions as a function of laser power at 21 °C (filled symbols), 28 °C (open blue symbols), and 34 °C (open red symbols). As these figures show, the diffusion coefficient remains constant across all laser powers for each samples within the error bars, but increases slightly with temperature. A constant fit yields a laser power-independent diffusion coefficient for each concentration and temperature. The resulting D_{meas} values are plotted as a function of concentration in Fig. 7.

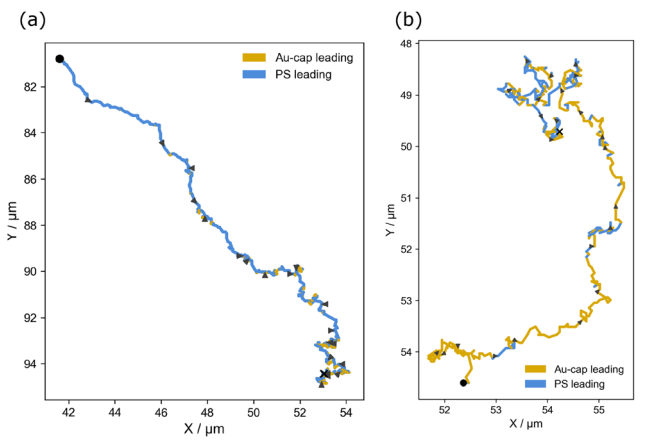

Fig. 6 (a) Direction of propulsion in water at 21 °C with the PS hemisphere leading, and (b) direction of propulsion in 0.05 wt% PNIPAM at 21 °C with the Au cap leading.

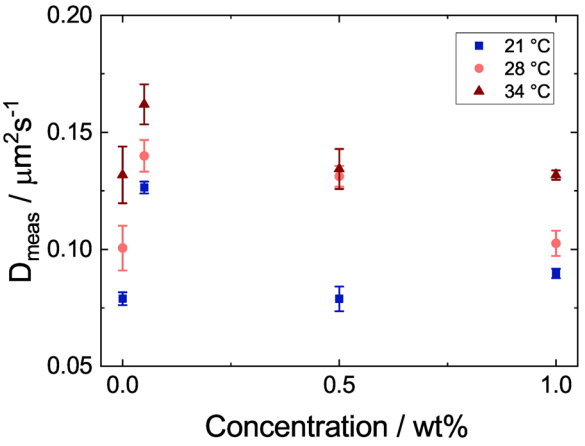

Fig. 7 Diffusion coefficients as a function of PNIPAM concentration. The blue squares represent 21 °C, the light red circles 28 °C, and the dark red triangles 34 °C.

For all concentrations, the diffusion coefficient increases with temperature. The lowest values are observed at 21 °C (blue squares), followed by higher values at 28 °C (light red circles), and the highest at 34 °C (dark red triangles). Adding PNIPAM slightly increases D_{meas} compared to water, but higher polymer concentrations result in a gradual decrease.

Reversibility

Fig. 8 shows the thermophoretic velocity (a) and the diffusion coefficients (b) in a 0.5 wt% PNIPAM solution as functions of laser power. The open blue symbols correspond to the measurements at 28 °C, while the light blue triangles represent values recorded at the same temperature after the sample had been heated to 34 °C. After heating to 34 °C, a slight reduction in the thermophoretic velocity and a pronounced decrease in the diffusion coefficient are observed. The dotted lines in Fig. 8(b) indicate the corresponding constant fits.

3.6 Temperature-dependent viscosity

Viscosities of water and the PNIPAM solutions were determined at discrete temperatures (20 °C, 28 °C, and 34 °C) using an Ubbelohde viscometer. Additional viscosity data obtained from rheometer measurements are provided in Fig. S9 in the SI. While the viscosities reported in Fig, S9 were measured with a rheometer at shear rates between 300–750 1 s^{-1}, these shear rates are significantly higher than those experienced by the surrounding fluid due to the motion of a Janus particle in the experiment. The effective shear rate induced by a moving particle can be roughly estimated as $\dot{\gamma} \approx v_{th}/R$, where v_{th} is the thermophoretic particle velocity and R the particle radius. For Janus particles with a diameter of 2.39 µm and velocities ranging from approximately 1 to 6 µm s^{-1}, the resulting local shear rates lie between 0.8 and 5 s^{-1}.

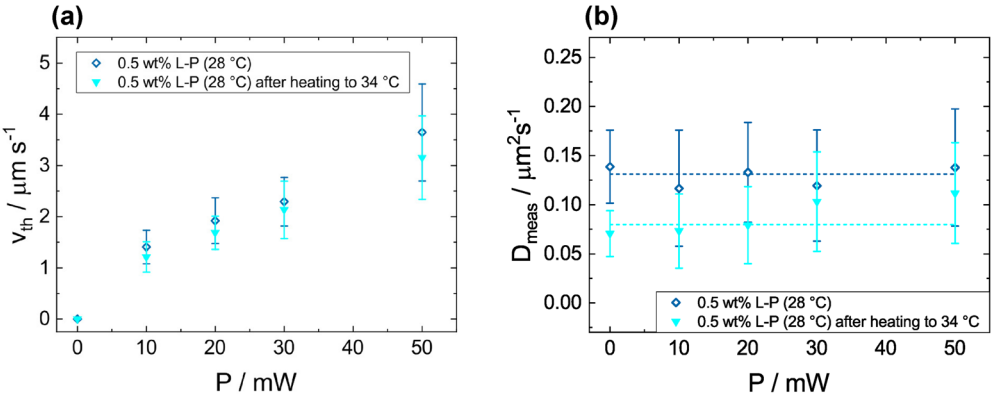

Fig. 8 (a) Thermophoretic velocity and (b) diffusion coefficients in a 0.5 wt% PNIPAM solution as functions of laser power at 28 °C (open blue diamonds) and at 28 °C after heating to 34 °C before (light blue triangles). The dotted lines in (b) indicate constant fits.

In contrast, the Ubbelohde viscometer allows estimation of the apparent shear rate at the capillary walls as $\dot{\gamma}_{wall} = 8v_{fluid}/d_{capillary}$,[60,61] where v_{fluid} is the average fluid velocity and $d_{capillary}$ = 0.63 mm is the capillary diameter. Using the measured flow times of 99.2 s for water and 146.4 s for 1 wt% PNIPAM, and a capillary length of approximately 10 cm, the resulting shear rates ($\dot{\gamma}_{wall}$ = 8.7–12.8 s^{-1}) are very close to the estimated shear rates induced by a single Janus particle in the surrounding medium.

The dynamic viscosities obtained from the Ubbelohde measurements are summarized in Table 1. These results confirm the trends observed with rotational rheometry. At 0.5 wt% and 1 wt% PNIPAM, measurements could not be obtained at 34 °C because the solutions did not flow through the capillary, likely due to partial blockage caused by polymer aggregation.

Overall, the viscosities of the PNIPAM solutions are similar to that of water, as measured either by rotational rheometry or the Ubbelohde viscometer.

Table 1 Dynamic viscosities measured with an Ubbelohde viscometer at selected temperatures

Solution	η (20 °C)/mPa s	η (28 °C)/mPa s	η (34 °C)/mPa s
MilliQ water	1.0121 ± 0.0001	0.82 ± 0.02	0.7542 ± 0.0003
0.05 wt% PNIPAM	1.05 ± 0.03	0.84 ± 0.03	0.77 ± 0.01
0.5 wt% PNIPAM	1.240 ± 0.002	1.00 ± 0.01	—
1 wt% PNIPAM	1.50 ± 0.01	1.170 ± 0.003	—

Discussion

Thermophoretic velocity

To understand the propulsion of Au–PS Janus particles in PNIPAM solutions, it is useful to first recall their behavior in simple fluids. In water, the particles move with the PS hemisphere forward, driven by self-thermophoresis: laser illumination heats the Au cap heats up, creating a temperature gradient across the particle. This gradient induces an asymmetric distribution of ions within the electric double layer (EDL). The resulting local interfacial gradient in ion concentration gives rise to thermo-electro-osmotic flows along the particle surface. Momentum exchange between these surface flows and the surrounding fluid propels the particles toward the colder PS hemisphere. As a result, the thermophoretic velocity increases linearly with laser power and remains largely independent of temperature, as observed in the reference measurements in water.

Direct momentum transfer from photon absorption (“radiation pressure”) can be excluded as a contributing mechanism to the observed propulsion, since it acts only along the optical axis, which is perpendicular to the propulsion direction. Moreover, radiation pressure is orders of magnitude too weak to generate the in-plane propulsion observed here.

The addition of PNIPAM fundamentally alters this balance by introducing a thermodiffusive solute whose transport properties vary sharply with temperature. According to Kita *et al.*,[56] linear PNIPAM exhibits a positive Soret coefficient S_T in aqueous solutions, meaning that the polymer chains migrate towards the colder region under a temperature gradient. Similar thermophoretic behavior has been reported for other PNIPAM-based systems: Königer *et al.*[62] demonstrated that thermo-sensitive core–shell particles with a PS core and PNIPAM shell possess a positive Soret coefficient, while Wongsuwarn *et al.*[63] likewise found that thermo-responsive PNIPAM microgel particles exhibit a positive S_T. At low PNIPAM concentrations, particularly around 0.05 wt%, local heating of the Au hemisphere induces a PNIPAM concentration gradient around the Janus particle, since the polymer migrates toward the cooler PS side due to its positive Soret coefficient. The gradient causes an entropic force (depletion force) pushing the Janus particle from high-to-low PNIPAM concentration, *i.e.*, from the cold PS side towards the hot Au cap. This generates an additional diffusiophoretic drift opposing its intrinsic thermophoretic motion.

The competition between these two effects explains the observed reversal of propulsion direction. At very low concentrations ($\leq$0.04 wt%), the thermophoretic contribution dominates, and the particle moves with the PS hemisphere forward, as in pure water. At slightly higher concentrations ($\geq$0.05 wt%), the polymer-induced diffusiophoretic drift becomes dominant

in magnitude, leading to motion with the Au cap facing forward. Importantly, the magnitude of the total velocity reaches a maximum near the LCST, where the Soret coefficient of PNIPAM peaks.

The theoretical calculations also explain the non-monotonic speed of the particle observed in the experiments at such low concentrations of PNIPAM. The calculated speed peaks at ≈ 9 μm s^{-1} around 31 °C, which is driven by the sharp peak in the Soret coefficient S_T at the LCST. Above the LCST, however, the Soret coefficient decreases, weakening the diffusiophoretic drift and lowering the overall particle speed. As a result, the thermophoretic component again becomes the stronger contribution, which can lead to a reversal of the propulsion direction back to PS-forward motion at high temperatures, as predicted for the 0.05 wt% solution.

At higher polymer concentrations (0.5 and 1 wt% PNIPAM) and elevated temperatures (34 °C), self-propulsion is no longer observed. The Janus particles exhibit purely Brownian motion under laser illumination. This suggests that polymer adsorption onto the particle surface becomes increasingly important. PNIPAM is known to adsorb on both Au[64–68] and PS[69,70] surfaces, and adsorption increases with temperature rises.[64,69] This adsorption could significantly weaken or even eliminate the temperature gradient at the particle surface or shield the electric double layer (EDL), thereby suppressing the thermo-electro-osmotic flow. A dense, collapsed PNIPAM layer at high temperatures and concentrations likely increases hydrodynamic drag and disrupts interfacial ion distributions, both effects that inhibit propulsion.

Evidence for polymer adsorption comes from post-heating measurements (see Fig. 8): the thermophoretic velocity is only slightly reduced at 28 °C after heating to 34 °C, but the diffusion coefficient decreases significantly, suggesting an increased effective particle radius. While higher viscosity could also contribute to this reduction in diffusion coefficient, the viscosity of the solution actually decreases upon cooling (see Fig. 8(b)), ruling it out as the primary cause. Zeta potential measurements of the Janus particles in water and in the PNIPAM solutions further support this interpretation: increasing PNIPAM concentration at a constant temperature reduces the absolute zeta potential of Janus particles, indicating stronger polymer adsorption that screens surface charge (see Table S3 in the SI for details). Upon heating from 20 °C to 40 °C, the absolute zeta potential further decreases, suggesting enhanced adsorption with temperature. Notably, after cooling back to 20 °C, the absolute zeta potential remains reduced compared to initial values, implying irreversible polymer adsorption on the particle surface.

Overall, the thermophoretic behavior of Janus particles in PNIPAM solutions emerges from a delicate balance between thermophoretic and diffusiophoretic, and adsorption-driven effects. The direction reversal and non-monotonic speed near the LCST directly reflect the temperature-dependent thermodiffusion of PNIPAM, demonstrating how molecular-scale polymer responses can reprogram the active behavior of colloidal microswimmers.

Diffusion coefficient

An increased diffusion coefficient with increasing temperature can be explained by several factors. First, as the temperature increases, the viscosity of the solution decreases and according to Fig. S9, $\eta(21\ ^\circ\mathrm{C}) > \eta(28\ ^\circ\mathrm{C}) > \eta(34\ ^\circ\mathrm{C})$ for all solutions. According to the Stokes–Einstein equation (eqn (2)), the diffusion coefficient of a spherical particle is inversely proportional to the viscosity. Additionally, higher temperatures provide more thermal energy, leading to an enhanced Brownian motion of the particle. For the PNIPAM solutions, the polymer molecules collapse above the LCST, which could lead to a reduced hydrodynamic hindrance of the particle.

The fact that D_{meas} is considerably smaller than D_{bulk} is consistent with findings reported in the literature.[14,51,71–73] The decrease in diffusion coefficient with increasing polymer concentration can be explained by several competing effects. First, at the lowest polymer concentration (0.05 wt%), the PNIPAM solution is in the dilute regime. This means that the individual polymer coils are well-separated, and their influence on the particle's motion is minimal. However, as the concentration increases towards 0.5 and 1 wt%, the solutions possibly enter the semi-dilute regime, where the polymer chains start to overlap. This could create a transient network that increases the viscoelastic resistance to the particle motion. The viscosity of the solution also increases with increasing polymer concentration, which generally slows down particle diffusion.

Temperature dependent viscosity

The viscosity of liquids, such as water, decreases with increasing temperature due to weakened intermolecular cohesive forces, which reduce internal resistance to flow.[74–78] Before examining the viscosity behavior of PNIPAM, it is essential to understand its temperature-responsive nature. Poly(*N*-isopropyl acrylamide) (PNIPAM) is a temperature-responsive polymer with a lower critical solution temperature (LCST) of around 31 °C[34]–32 °C[35–39] in aqueous solution. Below the LCST, PNIPAM exists as a hydrated, expanded coil stabilized by hydrogen bonding with water.[36,37,40,41] As the temperature increases, hydrogen bonds between PNIPAM and water weaken. This leads to partial dehydration and hydrophobic collapse into a globular structure, driven by intramolecular hydrogen bonding.[35–37,41] Above the LCST, hydrophobic interactions dominate, causing polymer aggregation and phase separation due to entropy-driven dehydration.[38,40,42,43] This reversible transition has been confirmed experimentally[36,37,39] and theoretically.[38,42,43] The temperature-dependent viscosity of the PNIPAM solutions exhibits a peak near the LCST, consistent with observations by Tam *et al.*,[79,80] Badiger *et al.*,[81] and Kelemen *et al.*[82] This behavior was divided into three regions, as described in Tam *et al.*[79,80] In region I, viscosity decreases with rising temperature as Brownian motion disrupts hydrogen-bonded ''water cages'', leading to chain collapse and a reduction in hydrodynamic volume. This trend reverses near the LCST. In region II, just before the LCST, viscosity rises as PNIPAM chains associate *via* hydrophobic interactions,

forming a transient network. This effect strengthens with increasing polymer concentration, enhancing the viscosity peak. Beyond the LCST (region III), PNIPAM undergoes phase separation, forming colloidal aggregates. This causes a sharp viscosity drop, stabilizing at a steady value, largely independent of polymer concentration.

In this study, the overlap concentration c^* was estimated to be above 0.49 wt%, placing the lowest concentration (0.05 wt%) in the dilute regime. In contrast, the medium (0.5 wt%) and highest (1 wt%) concentrations may be in the transition to the semi-dilute regime. Interestingly, a viscosity peak is observed even at 0.05 wt%, although Badiger *et al.*[81] reported that this peak vanishes below the overlap concentration. Notably, despite the significantly lower molecular weight of the polymer used in this chapter compared to that in their work, the polymer chains here still exhibit transient association near the LCST. This viscosity peak is also observed in other systems, such as PNIPAM microgel solutions[83–85] and interpenetrating polymer network nanoparticles.[86]

Near-newtonian behavior and its implications

It is worth noting that although elastic components of viscoelastic media can strongly affect active particle propulsion, as shown by Bechinger and coworkers,[87,88] the system investigated here behaves fundamentally differently. While their studies employed a binary mixture with a lower critical solution temperature (LCST) and added polymer, where heating induced phase separation and complex viscoelastic properties,[87,88] the PNIPAM solutions in this study are dilute, aqueous, and undergo a well-defined coil-to-globule transition. As a result, a direct comparison between the two systems is not straightforward. A key distinction lies in the viscosity regime: Gomez-Solano *et al.*[87] reported effective viscosities as high as 150 mPa s based on diffusional measurements. Following the same approach, viscosity values were calculated from the measured diffusion coefficients D_{meas} (*e.g.*, see Fig. 7) using the Stokes–Einstein equation (eqn (2)). These calculations yielded viscosities for the PNIPAM solutions that are remarkably close to those of pure water, ranging from 2.29 mPa s at 21 °C (for 0.5 wt% PNIPAM, lowest D_{meas}) to 1.16 mPa s at 28 °C (for 0.05 wt% PNIPAM, highest D_{meas}).

These diffusion-based estimates are in excellent agreement with the results obtained from two additional and independent methods. First, rotational rheometer measurements (performed at higher shear rates between approximately 300–750 1 s^{-1}), also yielded viscosity values within the same narrow range of about 0.7 to 1.6 mPa s. Second, measurements using an Ubbelohde viscometer confirmed similarly low viscosities. The strong agreement across all three approaches indicates that the PNIPAM solutions show negligible shear thinning under the conditions studied and behave essentially as Newtonian fluids. This observation can be attributed to the low polymer concentrations and the short chain lengths of the PNIPAM used in this thesis. These findings are further supported by earlier studies on PNIPAM solutions of similar concentrations. For example, Tam *et al.*[80] and Pamies *et al.*[89] found flat viscosity curves even at low shear rates, with the strongest shear thinning occurring only near the LCST. This general trend aligns well with flat viscosity profiles observed here and supports the assumption that the shear rates relevant to Janus particle motion do not significantly affect the local viscosity. These shear rates can be estimated as $\dot{\gamma} \approx v_{th}/R$, where v_{th} is the thermophoretic particle velocity and R the particle radius. For Janus particles with a diameter of 2.39 μm and velocities ranging from approximately 1 to 6 μm s^{-1}, the resulting local shear rates lie between 0.8 and 5 s^{-1}.

This main difference in viscosity places our system firmly in a regime much closer to Newtonian behavior, where elastic contributions are expected to be minimal. In agreement with this, no changes in rotational diffusion were observed that would suggest elastic effects. This is in contrast to the findings of Bechinger and coworkers, where active motion was strongly affected by the elastic component, resulting in faster reorientation at higher velocities and persistent rotational motion.[87,88] Finally, although the viscosity of water decreases from 0.99 mPa s at 21 °C to 0.75 mPa s at 34 °C, no corresponding change in the thermophoretic velocity of the Janus particles was observed, suggesting that propulsion is not primarily governed by such modest viscosity variations.

Despite the close match between the viscosity of these polymer solutions and that of pure water, a significant increase in thermophoretic velocity was observed with increasing temperature (at 28 °C) at low polymer concentrations (0.05 wt%). The reasons for this enhancement will be discussed in the next section.

Conclusion

This study demonstrates that the thermophoretic velocity of Au–PS Janus particles can be effectively tuned by adding the temperature-responsive polymer PNIPAM into the surrounding fluid. Both temperature and polymer concentration critically influence particle propulsion through a combination of thermophoretic, diffusiophoretic, and adsorption-driven effects.

In pure water, Au–PS Janus particles propel with the PS side forward because their intrinsic thermophoretic motion drives them toward the cooler hemisphere. At low PNIPAM concentration (0.05 wt%), both experiments and theoretical calculations show a non-monotonic temperature dependence of the propulsion speed. As the temperature increases from 21 °C to 28 °C, the speed rises and reaches a maximum just below the LCST. In this regime, PNIPAM has a positive Soret coefficient, causing the polymer to accumulate near the cooler PS hemisphere. The resulting polymer concentration gradient generates an additional diffusiophoretic drift that dominates over the intrinsic thermophoretic velocity, enhancing the particle speed and even reversing its propulsion direction. Above the LCST, the Soret coefficient drops, the depletion-induced drift weakens, and the thermophoretic contribution becomes dominant again, consistent with the experimentally observed direction reversal and lower speed at higher temperatures in 0.05 wt% PNIPAM solutions. Despite the good agreement between

experiments and theoretical predictions, we stress that the self-thermophoretic motion of our Janus particles in PNIPAM gradients will generally depend on many different factors[58,90] (particularly at higher PNIPAM concentration) that we shall explore in more detail in future works.

Despite the presence of PNIPAM, diffusion-based calculations, rotational rheometry, and Ubbelohde viscometry all confirm that the PNIPAM solutions exhibit viscosities very close to that of pure water and show no significant shear thinning. This near Newtonian behavior ensures that elastic contributions to particle motion remain minimal, as supported by the absence of rotational diffusion anomalies. These findings confirm that the observed changes in propulsion are not governed by viscosity, but rather by polymer structure and interfacial effects.

At higher PNIPAM concentrations ($\geq$0.5 wt%), stronger polymer adsorption on the particle surface dampens temperature gradients and suppresses thermophoretic motion. Above the LCST, only Brownian motion is observed. Importantly, some adsorption effects appear irreversible and persist even after cooling. This is evidenced by reduced zeta potentials and lowered diffusion coefficients, suggesting a permanent increase in effective particle size due to adsorbed polymer. Meanwhile, the diffusion coefficient increases with temperature but decreases slightly with polymer concentration, consistent with increased solution viscosity and polymer adsorption increasing the effective particle size.

Overall, these findings highlight that the self-propulsion of Au–PS Janus particles in temperature-sensitive PNIPAM solutions is governed by a delicate interplay between thermophoresis, polymer-induced diffusiophoresis, and adsorption effects. By fine-tuning these parameters, it is possible to either enhance, suppress, or even reverse particle propulsion, which could be relevant for applications in microscale transport, drug delivery, and active matter systems. Future studies could further explore the role of particle surface interactions and temperature gradients to optimize control over active particle dynamics in complex fluids.

Author contributions

All authors have given approval to the final version of the manuscript.

Conflicts of interest

The authors declare no competing financial interest.

Data availability

The data that supports the findings of this study are available in the supplementary information (SI) of this article. Supplementary information: parameters of the coating process; SEM image of Janus particle with corresponding EDX analysis image; mean squared displacement (MSD) curves of all particles at different laser intensities with corresponding trajectories in the *xy*-plane; diffusion coefficients of all samples as function of laser power; temperature-dependent viscosity of all samples; viscosity as a function of shear rate; kinematic viscosity values; ν_{th} at 28 °C and at 28 °C after heating to 34 °C: zeta potential values (PDF). See DOI: https://doi.org/10.1039/d5sm01119a.

Acknowledgements

The study is funded by the Deutsche Forschungsgemeinschaft (DFG, German Research Foundation) – project number 509491635, *via* the Research Unit ''Transient Sieves'', FOR 5584 (research projects A2 and B1), and the collaborative research center Multiscale Simulation Methods for Soft-Matter Systems, TRR 146 (Project No. 233630050). The authors would like to express their gratitude to Dominik Richter (group of Prof. Dr Annette Andrieu-Brunsen, Chemistry Department Technical University of Darmstadt (Germany)) for his help with the thermal evaporation of the Janus particles in their thermal evaporator CREAMET 300 V2. We sincerely thank Dr Michael Wagner (Materials Science Department, GSI Darmstadt, Germany) for his valuable assistance with the SEM and EDX measurements and Prof. Dr Maria Eugenia Toimil-Molares (Materials Science Department, GSI Darmstadt, Germany) for providing access to the Gemini 500 Field Emission Scanning Electron Microscope. Sincere thanks also to Carina Schneider for conducting the Zetasizer measurements and to Sierk Lessnau for preparing some of the PNIPAM solutions. The authors also thank Dr Olaf Soltwedel (Institute for Condensed Matter Physics, Technical University of Darmstadt, Germany) for fruitful discussions.

References

1 A. Walther, M. Hoffmann and A. H. E. Müller, Emulsion Polymerization Using Janus Particles as Stabilizers, *Angew. Chem., Int. Ed.*, 2008, **47**, 711–714.
2 R. Aveyard, Can Janus particles give thermodynamically stable Pickering emulsions?, *Soft Matter*, 2012, **8**, 5233–5240.
3 A. Kirillova, C. Marschelke, J. Friedrichs, C. Werner and A. Synytska, Hybrid Hairy Janus Particles as Building Blocks for Antibiofouling Surfaces, *ACS Appl. Mater. Interfaces*, 2016, **8**, 32591–32603.
4 S. Campuzano, M. Gamella, V. Serafñn, M. Pedrero, P. Yáñez-Sedeño and J. M. Pingarrón, Magnetic Janus Particles for Static and Dynamic (Bio)Sensing, *Magnetochemistry*, 2019, **5**, 47.
5 C. Liu, J. Huang, T. Xu and X. Zhang, Powering bioanalytical applications in biomedicine with light-responsive Janus micro-/nanomotors, *Microchim. Acta*, 2022, **189**, 116.
6 D. Kagan, R. Laocharoensuk, M. Zimmerman, C. Clawson, S. Balasubramanian, D. Kang, D. Bishop, S. Sattayasamitsathit, L. Zhang and J. Wang, Rapid Delivery of Drug Carriers Propelled

and Navigated by Catalytic Nanoshuttles, *Small*, 2010, **6**, 2741–2747.
7 L. Baraban, M. Tasinkevych, M. N. Popescu, S. Sanchez, S. Dietrich and O. G. Schmidt, Transport of cargo by catalytic Janus micro-motors, *Soft Matter*, 2012, **8**, 48–52.
8 A. F. Demirörs, M. T. Akan, E. Poloni and A. R. Studart, Active cargo transport with Janus colloidal shuttles using electric and magnetic fields, *Soft Matter*, 2018, **14**, 4741–4749.
9 S. Erez, E. Karshalev, Y. Wu, J. Wang and G. Yossifon, Electrical Propulsion and Cargo Transport of Microbowl Shaped Janus Particles, *Small*, 2022, **18**, 2101809.
10 J. R. Howse, R. A. L. Jones, A. J. Ryan, T. Gough, R. Vafabakhsh and R. Golestanian, Self-Motile Colloidal Particles: From Directed Propulsion to Random Walk, *Phys. Rev. Lett.*, 2007, **99**, 048102.
11 Z. Jalilvand, A. B. Pawar and I. Kretzschmar, Experimental Study of the Motion of Patchy Particle Swimmers Near a Wall, *Langmuir*, 2018, **34**, 15593–15599.
12 W. F. Paxton, K. C. Kistler, C. C. Olmeda, A. Sen, S. K. St. Angelo, Y. Cao, T. E. Mallouk, P. E. Lammert and V. H. Crespi, Catalytic Nanomotors: Autonomous Movement of Striped Nanorods, *J. Am. Chem. Soc.*, 2004, **126**, 13424–13431.
13 H.-R. Jiang, N. Yoshinaga and M. Sano, Active Motion of a Janus Particle by Self-Thermophoresis in a Defocused Laser Beam, *Phys. Rev. Lett.*, 2010, **105**, 268302.
14 M. Heidari, F. Jakob, B. Liebchen and R. von Klitzing, Non-monotonic speed-dependence of microswimmers on wall distance, *Soft Matter*, 2021, **17**, 9428–9433.
15 F. Braun, M. F. P. Wagner, M. E. Toimil-Molares and R. von Klitzing, Comparison of Different Preparation Techniques of Thermophoretic Swimmers and Their Propulsion Velocity, *Langmuir*, 2024, **40**, 5606–5616.
16 A. P. Bregulla and F. Cichos, Flow fields around pinned self-thermophoretic microswimmers under confinement, *J. Chem. Phys.*, 2019, **151**(4).
17 A. P. Bregulla and F. Cichos, Size dependent efficiency of photophoretic swimmers, *Faraday Discuss.*, 2015, **184**, 381–391.
18 G. Li, E. Lauga and A. M. Ardekani, Microswimming in viscoelastic fluids, *J. Non-Newtonian Fluid Mech.*, 2021, **297**, 104655.
19 B. Liu, T. R. Powers and K. S. Breuer, Force-free swimming of a model helical flagellum in viscoelastic fluids, *Proc. Natl. Acad. Sci. U. S. A.*, 2011, **108**, 19516–19520.
20 G. Natale, C. Datt, S. G. Hatzikiriakos and G. J. Elfring, Autophoretic locomotion in weakly viscoelastic fluids at finite Péclet number, *Phys. Fluids*, 2017, **29**, 123102.
21 H. Raman, S. Das, H. Sharma, K. Singh, S. Gupta and R. Mangal, Dynamics of Active SiO2–Pt Janus Colloids in Dilute Poly(ethylene oxide) Solutions, *ACS Phys. Chem. Au*, 2023, **3**, 279–289.
22 N. Samanta, R. Goswami and R. Chakrabarti, Diffusion of self-propelled Janus tracer in polymeric environment, 2017, https://arxiv.org/abs/1704.06207.
23 R. S. Yadav, C. Das and R. Chakrabarti, Dynamics of a spherical self-propelled tracer in a polymeric medium: interplay of self-propulsion, stickiness, and crowding, *Soft Matter*, 2023, **19**, 689–700.
24 W. R. Schneider and R. N. Doetsch, Effect of Viscosity on Bacterial Motility, *J. Bacteriol.*, 1974, **117**, 696–701.
25 H. Berg and L. Turner, Movement of microorganisms in viscous environments, *Nature*, 1979, **278**, 349–351.
26 Y. Magariyama and S. Kudo, A Mathematical Explanation of an Increase in Bacterial Swimming Speed with Viscosity in Linear-Polymer Solutions, *Biophys. J.*, 2002, **83**, 733–739.
27 V. A. Martinez, J. Schwarz-Linek, M. Reufer, L. G. Wilson, A. N. Morozov and W. C. K. Poon, Flagellated bacterial motility in polymer solutions, *Proc. Natl. Acad. Sci. U. S. A.*, 2014, **111**, 17771–17776.
28 A. Patteson, A. Gopinath, M. Goulian and P. E. Arratia, Running and tumbling with *E. coli* in polymeric solutions, *Sci. Rep.*, 2015, **5**, 15761.
29 D. J. Smith, E. A. Gaffney, H. GadÃ♀lha, N. Kapur and J. C. Kirkman-Brown, Bend propagation in the flagella of migrating human sperm, and its modulation by viscosity, *Cell Motility*, 2009, **66**, 220–236.
30 J. Teran, L. Fauci and M. Shelley, Viscoelastic Fluid Response Can Increase the Speed and Efficiency of a Free Swimmer, *Phys. Rev. Lett.*, 2010, **104**, 038101.
31 S. Sahoo, S. P. Singh and S. Thakur, Role of viscoelasticity on the dynamics and aggregation of chemically active sphere-dimers, *Phys. Fluids*, 2021, **33**, 017120.
32 A. M. Leshansky, Enhanced low-Reynolds-number propulsion in heterogeneous viscous environments, *Phys. Rev. E: Stat., Nonlinear, Soft Matter Phys.*, 2009, **80**, 051911.
33 D. Schamel, A. G. Mark, J. G. Gibbs, C. Miksch, K. I. Morozov, A. M. Leshansky and P. Fischer, Nanopropellers and Their Actuation in Complex Viscoelastic Media, *ACS Nano*, 2014, **8**, 8794–8801.
34 M. Heskins and J. E. Guillet, Solution Properties of Poly(*N*-isopropylacrylamide), *J. Macromol. Sci., Part A: Pure Appl. Chem.*, 1968, **2**, 1441–1455.
35 G. Graziano, On the temperature-induced coil to globule transition of poly-*N*-isopropylacrylamide in dilute aqueous solutions, *Int. J. Biol. Macromol.*, 2000, **27**, 89–97.
36 Z. Ahmed, E. A. Gooding, K. V. Pimenov, L. Wang and S. A. Asher, UV Resonance Raman Determination of Molecular Mechanism of Poly(N-isopropylacrylamide) Volume Phase Transition, *J. Phys. Chem. B*, 2009, **113**, 4248–4256.
37 I. Juurinen, S. Galambosi, A. G. Anghelescu-Hakala, J. Koskelo, V. Honkimäki, K. Hämäläinen, S. Huotari and M. Hakala, Molecular-Level Changes of Aqueous Poly(N-isopropylacrylamide) in Phase Transition, *J. Phys. Chem. B*, 2014, **118**, 5518–5523.
38 L. J. Abbott, A. K. Tucker and M. J. Stevens, Single Chain Structure of a Poly(N-isopropylacrylamide) Surfactant in Water, *J. Phys. Chem. B*, 2015, **119**, 3837–3845.
39 C. G. Lopez, A. Scotti, M. Brugnoni and W. Richtering, The Swelling of Poly(Isopropylacrylamide) Near the ϑ Temperature:

A Comparison between Linear and Cross-Linked Chains, *Macromol. Chem. Phys.*, 2019, **220**, 1800421.
40 H. Schild, Poly(N-isopropylacrylamide): experiment, theory and application, *Prog. Polym. Sci.*, 1992, **17**, 163–249.
41 M. Podewitz, Y. Wang, P. K. Quoika, J. R. Loeffler, M. Schauperl and K. R. Liedl, Coil-Globule Transition Thermodynamics of Poly(N-isopropylacrylamide), *J. Phys. Chem. B*, 2019, **123**, 8838–8847.
42 S. A. Deshmukh, S. K. R. S. Sankaranarayanan, K. Suthar and D. C. Mancini, Role of Solvation Dynamics and Local Ordering of Water in Inducing Conformational Transitions in Poly(N-isopropylacrylamide) Oligomers through the LCST, *J. Phys. Chem. B*, 2012, **116**, 2651–2663.
43 S. A. Deshmukh, G. Kamath, K. J. Suthar, D. C. Mancini and S. K. R. S. Sankaranarayanan, Non-equilibrium effects evidenced by vibrational spectra during the coil-to-globule transition in poly(N-isopropylacrylamide) subjected to an ultrafast heating–cooling cycle, *Soft Matter*, 2014, **10**, 1462–1480.
44 I. R. Peterson, Langmuir–Blodgett films, *J. Phys. D: Appl. Phys.*, 1990, **23**, 379–395.
45 L. Zhi-cheng, R. Wei-dong, J. Nan, R. Lu-quan, C. Qian and Z. Bing, Fabrication of Large-scale Nanostructure by Langmuir-Blodgett Technique, *J. Bionic Eng.*, 2006, **3**, 59–62.
46 T. Bickel, A. Majee and A. Würger, Flow pattern in the vicinity of self-propelling hot Janus particles, *Phys. Rev. E: Stat., Nonlinear, Soft Matter Phys.*, 2013, **88**, 012301.
47 M. Heidari, A. Bregulla, S. M. Landin, F. Cichos and R. von Klitzing, Self-Propulsion of Janus Particles near a Brush-Functionalized Substrate, *Langmuir*, 2020, **36**, 7775–7780.
48 G. E. Uhlenbeck and L. S. Ornstein, On the Theory of the Brownian Motion, *Phys. Rev.*, 1930, **36**, 823–841.
49 K. Martens, L. Angelani, R. Di Leonardo and L. Bocquet, Probability distributions for the run-and-tumble bacterial dynamics: an analogy to the Lorentz model, *Eur. Phys. J. E: Soft Matter Biol. Phys.*, 2012, **35**, 84.
50 S. Ketzetzi, J. de Graaf and D. J. Kraft, Diffusion-Based Height Analysis Reveals Robust Microswimmer-Wall Separation, *Phys. Rev. Lett.*, 2020, **125**, 238001.
51 B. Lin, J. Yu and S. A. Rice, Diffusion of an isolated colloidal sphere confined between flat plates, *Colloids Surf., A*, 2000, **174**, 121–131.
52 A. Fahr, *Voigt's pharmaceutical technology*, John Wiley & Sons, 2018.
53 G. Stachowiak and A. W. Batchelor, *Engineering tribology*, Butterworth-heinemann, 2025.
54 W.-F. Pu, R. Liu, B. Li, F.-Y. Jin, Q. Peng, L. Sun, D.-J. Du and F.-S. Yao, Amphoteric hyperbranched polymers with multistimuli-responsive behavior in the application of polymer flooding, *RSC Adv.*, 2015, **5**, 88002–88013.
55 H.-R. Jiang, H. Wada, N. Yoshinaga and M. Sano, Manipulation of Colloids by a Nonequilibrium Depletion Force in a Temperature Gradient, *Phys. Rev. Lett.*, 2009, **102**, 208301.
56 R. Kita and S. Wiegand, Soret coefficient of poly(N-isopropylacrylamide)/water in the vicinity of coil-globule transition temperature, *Macromolecules*, 2005, **38**, 4554–4556.
57 M. Fränzl and F. Cichos, Hydrodynamic Manipulation of Nano-Objects by Optically Induced Thermo-Osmotic Flows, *Nat. Commun.*, 2022, **13**, 656.
58 A. Würger, Thermal Non-Equilibrium Transport in Colloids, *Rep. Prog. Phys.*, 2010, **73**, 126601.
59 E. J. Avital and T. Miloh, Self-Thermophoresis of Laser-Heated Spherical Janus Particles, *Eur. Phys. J. E: Soft Matter Biol. Phys.*, 2021, **44**, 139.
60 W. H. Herschel, On the rate of shear in capillary tubes, *J. Rheol.*, 1930, **1**, 505–506.
61 K. T. Trinh, The wall shear rate in non-Newtonian turbulent pipe flow, arXiv, 2010, preprint arXiv:1009.3299, DOI: 10.48550/arXiv.1009.3299.
62 A. Königer, N. Plack, W. Köhler, M. Siebenbürger and M. Ballauff, Thermophoresis of thermoresponsive polystyrene-poly(N-isopropylacrylamide) core-shell particles, *Soft Matter*, 2013, **9**, 1418–1421.
63 S. Wongsuwarn, D. Vigolo, R. Cerbino, A. M. Howe, A. Vailati, R. Piazza and P. Cicuta, Giant thermophoresis of poly(N-isopropylacrylamide) microgel particles, *Soft Matter*, 2012, **8**, 5857–5863.
64 M. A. Plunkett, Z. Wang, M. W. Rutland and D. Johannsmann, Adsorption of pNIPAM Layers on Hydrophobic Gold Surfaces, Measured in Situ by QCM and SPR, *Langmuir*, 2003, **19**, 6837–6844.
65 E. C. Cho, Y. D. Kim and K. Cho, Thermally responsive poly(N-isopropylacrylamide) monolayer on gold: synthesis, surface characterization, and protein interaction/adsorption studies, *Polymer*, 2004, **45**, 3195–3204.
66 E. J. Park, D. D. Draper and N. T. Flynn, Adsorption and Thermoresponsive Behavior of Poly(*N*-isopropylacrylamide-*co*-*N*,*N*-cystaminebisacrylamide) Thin Films on Gold, *Langmuir*, 2007, **23**, 7083–7089.
67 B. Wu, K. Wu, P. Wang and D.-M. Zhu, Adsorption Kinetics and Adsorption Isotherm of Poly(N-isopropylacrylamide) on Gold Surfaces Studied Using QCM-D, *J. Phys. Chem. C*, 2007, **111**, 1131–1135.
68 K. Wu, B. Wu, P. Wang, Y. Hou, G. Zhang and D.-M. Zhu, Adsorption Isotherms and Dissipation of Adsorbed Poly(N-isopropylacrylamide) in Its Swelling and Collapsed States, *J. Phys. Chem. B*, 2007, **111**, 8723–8727.
69 J. Gao and C. Wu, The ''coil-to-globule'' transition of poly(N-isopropylacrylamide) on the surface of a surfactant-free polystyrene nanoparticle, *Macromolecules*, 1997, **30**, 6873–6876.
70 J. G. Tengjiao Hu and C. Wu, Swelling and Shrinking of Poly(N-Isopropylacrylamide) Chains Adsorbed on the Surface of Polystyrene Nanoparticles, *J. Macromol. Sci., Part B: Phys.*, 2000, **39**, 407–414.
71 M. A. Bevan and D. C. Prieve, Hindered diffusion of colloidal particles very near to a wall: Revisited, *J. Chem. Phys.*, 2000, **113**, 1228–1236.
72 K. Kihm, A. Banerjee, C. Choi and T. Takagi, Near-wall hindered Brownian diffusion of nanoparticles examined

by three-dimensional ratiometric total internal reflection fluorescence microscopy (3-D R-TIRFM), *Exp. Fluids*, 2004, **37**, 811–824.
73 R. Schachoff, M. Selmke, A. Bregulla, F. Cichos, D. Rings, D. Chakraborty, K. Kroy, K. Günther, A. Henning-Knechtel and E. Sperling, Hot Brownian motion and photophoretic self-propulsion, *Diffusion Fundam.*, 2015, **23**, 1–19.
74 L. Korson, W. Drost-Hansen and F. J. Millero, Viscosity of water at various temperatures, *J. Phys. Chem.*, 1969, **73**, 34–39.
75 A. Nagashima, Viscosity of water substance-new international formulation and its background, *J. Phys. Chem. Ref. Data*, 1977, **6**, 1133–1166.
76 J. Kestin, M. Sokolov and W. A. Wakeham, Viscosity of liquid water in the range −8 °C to 150 °C, *J. Phys. Chem. Ref. Data*, 1978, **7**, 941–948.
77 H. Khodadadi, D. Toghraie and A. Karimipour, Effects of nanoparticles to present a statistical model for the viscosity of MgO–Water nanofluid, *Powder Technol.*, 2019, **342**, 166–180.
78 S. T. Pham and B. N. A. Nguyen, Application of the Finite Element Method Using Cohesive Elements to Model the Effect of Temperature, Rock Mechanical Properties, Fluid Injection Rate, and Fluid Properties on the Development of Hydraulic Fracture Height, *Modell. Simul. Eng.*, 2022, **2022**, 7413457.
79 K. Tam, X. Wu and R. Pelton, Viscometry—a useful tool for studying conformational changes of poly(N-isopropylacrylamide) in solutions, *Polymer*, 1992, **33**, 436–438.
80 K. C. Tam, X. Y. Wu and R. H. Pelton, Poly(N-isopropylacrylamide). II. Effect of polymer concentration, temperature, and surfactant on the viscosity of aqueous solutions, *J. Polym. Sci., Part A: Polym. Chem.*, 1993, **31**, 963–969.
81 M. V. Badiger and B. A. Wolf, Shear Induced Demixing and Rheological Behavior of Aqueous Solutions of Poly(N-isopropylacrylamide), *Macromol. Chem. Phys.*, 2003, **204**, 600–606.
82 K. Kelemen, R. Engel, L. L. Hecht, H. P. Schuchmann and C. Holtze, Influence of a Nonionic Surfactant on the Preparation of Polymer Dispersions by Precipitation Under Shear, *Macromol. Mater. Eng.*, 2013, **298**, 235–240.
83 A. M. Howe, S. Desrousseaux, L. S. Lunel, J. Tavacoli, H. N. Yow and A. F. Routh, Anomalous viscosity jump during the volume phase transition of poly(N-isopropylacrylamide) particles, *Adv. Colloid Interface Sci.*, 2009, **147–148**, 124–131, Colloids, polymers and surfactants.Special Issue in honour of Brian Vincent.
84 S. Franco, E. Buratti, V. Nigro, E. Zaccarelli, B. Ruzicka and R. Angelini, Glass and Jamming Rheology in Soft Particles Made of PNIPAM and Polyacrylic Acid, *Int. J. Mol. Sci.*, 2021, **22**, 4032.
85 V. Nigro, R. Angelini, M. Bertoldo, E. Buratti, S. Franco and B. Ruzicka, Chemical-Physical Behaviour of Microgels Made of Interpenetrating Polymer Networks of PNIPAM and Poly(acrylic Acid), *Polymers*, 2021, **13**, 1353.
86 X. Xia, Z. Hu and M. Marquez, Physically bonded nanoparticle networks: a novel drug delivery system, *J. Controlled Release*, 2005, **103**, 21–30.
87 J. R. Gomez-Solano, A. Blokhuis and C. Bechinger, Dynamics of Self-Propelled Janus Particles in Viscoelastic Fluids, *Phys. Rev. Lett.*, 2016, **116**, 138301.
88 N. Narinder, C. Bechinger and J. R. Gomez-Solano, Memory-induced transition from a persistent random walk to circular motion for achiral microswimmers, *Phys. Rev. Lett.*, 2018, **121**, 078003.
89 R. Pamies, K. Zhu, A.-L. Kjøniksen and B. Nyström, Thermal response of low molecular weight poly-(N-isopropylacrylamide) polymers in aqueous solution, *Polym. Bull.*, 2009, **62**, 487–502.
90 R. Piazza and A. Parola, Thermophoresis in Colloidal Suspensions, *J. Phys.: Condens. Matter*, 2008, **20**, 153102.

